Efficient single-photon extraction from quantum-dots embedded in GaAs micro-pyramids

Daniel Rülke,[a] Daniel M. Schaadt,[b] Heinz Kalt, and Michael Hetterich
Institut für Angewandte Physik and DFG Center for Functional Nanostructures (CFN), Karlsruhe Institute of Technology (KIT), Wolfgang-Gaede-Str. 1, 76131 Karlsruhe, Germany

(Received 4 May 2012; accepted 31 May 2012; published online 18 June 2012)

We demonstrate an easy method to fabricate efficient single-photon sources based on In(Ga)As quantum-dots embedded in reversed GaAs micro-pyramids. It relies on a single wet-chemical etching step utilizing an AlAs sacrificial layer. Due to the pyramidal shape of the cavities, we have been able to separate a small number of quantum-dots from the self-assembled ensemble and improve the extraction efficiency for single photons. The latter is predicted by finite difference time domain and finite elements method simulations to be about 80%–90% over a broad spectral range of 40 nm. Single-photon emission has been proven experimentally by means of auto-correlation measurements.
 [http://dx.doi.org/10.1063/1.4729482]

In recent years, many efforts have been devoted to the development of reliable single-photon sources on the basis of In(Ga)As semiconductor quantum dots (QDs) (e.g., Refs. 1 and 2, and references therein). Their non-classical light emission is an intrinsic property without any need for further improvements, but separation of single QDs as well as the collection efficiency of emitted light are two major issues that have been in focus of many researchers in this field. In order to improve the collection probability of emitted photons, the most common approach has been to embed the QDs into a resonant cavity sandwiched between two distributed Bragg reflectors (DBRs). After some structuring processes, the QD emission within a certain solid angle can be coupled out very efficiently if it is in resonance with this cavity. This resonant emission is enhanced compared to emission into leaky modes by the Purcell effect. Thereby, emission into the latter is effectively suppressed, but suppression is limited by the achievable Purcell enhancement.[2] Moreover, fulfilling the resonance condition for the QD emission is typically highly statistical, even if the emission wavelength can be tuned to some extent by temperature[3] and electric or magnetic fields.[4–6] For separation of single QDs, either low-density self-assembled or site-controlled[7,8] QD layers have been grown. Though site-controlling promised most reliable results, the quality, especially for single-photon generation, is still not competitive with self-assembled QDs despite recent improvements.[9]

In our work, we present an alternative approach that relies on embedding of QDs into reversed GaAs micro-pyramids (Fig. 1). Such geometry comes with a couple of benefits compared to planar cavities. The small cross-section of the pyramid close to its tip strongly reduces the number of QDs in the cavity if the QD layer is situated at this position. Thus, it is possible to easily separate single QDs from the self-assembled ensemble. The QD emission is mostly prevented from being lost into the substrate due to reflections at the facets and is not bound to a narrow resonance condition. Requirements of the molecular-beam epitaxial growth are low, particularly compared to DBR growth where high operation stability is always an issue for the long growth time and large amounts of source material which must be spent. The underlying wet-chemical fabrication process allows control over nearly every geometrical parameter as long as it is compatible with the crystal structure, as briefly described below. For a detailed description of the fabrication process, see previous publications.[10–13]

Initially, the height of the cavity and the position of the QD layer are set during molecular-beam epitaxial growth. The tip of the final pyramid will be located where a 70–120 nm AlAs sacrificial layer is grown. Thus, the distance of the QDs (20–100 nm) to this layer and the thickness (0.25–1.5 μm) of the GaAs layer above determine the position of the QD layer in the pyramid and the height of the pyramid, respectively. Before the etching process, a square or octagonal etching mask is exposed by standard e-beam lithography. The borders are oriented with respect to the crystallographic planes along the $\langle 100 \rangle$ and/or $\langle 110 \rangle$ directions. The subsequent wet-chemical etching process is performed with a solution of H_3PO_4, H_2O_2, and H_2O. Since the sacrificial layer is etched faster in this solution than GaAs, a controlled facet formation occurs as soon as this layer is reached. In Fig. 2, this behaviour is demonstrated with the results of a simulation that relies on a master equation approach for the propagation of the etching front. When fixing the ratio of phosphoric acid and water in the etchant, the

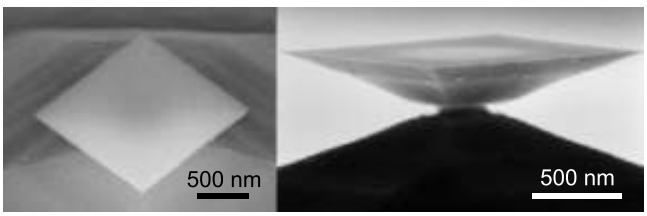

FIG. 1. Scanning electron micrographs of reversed micro-pyramid of 267 nm height and a facet angle of 30°.

[a]E-mail: daniel.ruelke@kit.edu.
[b]Present address: The Institute for Energy Research and Physical Technologies, Clausthal University of Technology, Am Stollen 19B, 38640 Goslar, Germany.

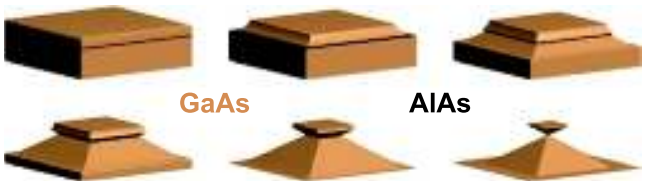

FIG. 2. Simulation of GaAs micro-pyramid formation during wet-chemical etching using a master equation approach. Due to the higher etching rate in the AlAs sacrificial layer, the facet formation occurs.

ratio as well as the two etching rates can be varied by the portion of hydrogen peroxide. Depending directly on the ratio of the etching rates, the facet angle can be adjusted in a range between 25° and 60°, too.

Since a direct comparison of the collection efficiency from QDs embedded in bulk GaAs and in cavities is quite difficult to realize due to the separation of single QDs in the cavities in contrast to ensemble emission from the bulk, we performed 3D finite difference time domain (FDTD) simulations and 2D finite elements method (FEM) simulations for transient propagation in order to receive more quantitative results on the out-coupling capabilities of the pyramidal cavities. To this end, a single monochromatic point source was situated in the cavity instead of a QD and the electromagnetic energy E_i that flows during a time interval $[t_s, t_e]$ through each of the six surfaces σ_i of a rectangular box (Fig. 3(a)) around the cavity were calculated by

$$E_i = \int_{t_s}^{t_e} \int_{\sigma_i} \vec{S}(\vec{r}, t) \cdot \mathrm{d}\vec{\sigma}_i \, \mathrm{d}t,$$

with the Poynting vector $\vec{S}(\vec{r}, t)$ and the surface normals $\vec{\sigma}_i$ pointing out of the computational domain. In the case of FDTD simulations, the calculation was started after a time t_s when a steady state had been established. The part of the emission that flows through surfaces σ_i can then be obtained by the normalized power flow $p_i = E_i / \sum_j E_j$. For the bottom surface, this is the part of emission that is lost into the GaAs substrate, while for the residual, it corresponds to the part that is radiated from the cavity into vacuum (Fig. 3). The dipole emitter was polarized perpendicular to the growth direction as expected for an excitonic interband transition in self-assembled InAs QDs.[14] In Fig. 3, the spectral dependency of the out-coupling efficiency and a sketch of the radiation profile with logarithmic color scale are shown. The simulation results demonstrate the broad spectral range of 900–940 nm in which the cavities can operate with out-coupling efficiencies between about 80% and 90%. The inset in Fig. 3(a) illustrates the directionality of the radiation by the logarithmic time-integrated field energy. This can be quantified roughly by the power flow through the top surface of 58%–76% in FDTD and 68%–76% in FEM simulations over the same spectral range.

Optical characterization of the cavities has been performed using micro-photoluminescence (μ-PL) utilizing an attached Hanbury–Brown and Twiss (HBT) set-up. The samples were excited with a continuous wave (cw) titanium:sapphire laser at around 830 nm. Their luminescence was dispersed in a 0.85 m double monochromator with two output slits behind the first and second grating, respectively. At the first slit, the output was focussed into a fiber splitter that directs to two silicon single-photon avalanche diodes (SPADs). Behind the second output, a silicon CCD was mounted for observation of a broader part of the spectrum. Having focussed onto a well distinct QD emission line, its excitonic nature was determined by means of the excitation power-dependency of the luminescence intensity. In order to be sure of measuring only a single QD line, the second order temporal correlation $g^{(2)}(\tau)$ of the emission was measured using the HBT set-up.

The graphs in Figs. 4 and 5 demonstrate the emission characteristics of a QD embedded at a level of 25 nm above the sacrificial layer in a pyramid of 500 nm height. The clear separation of a single QD line was observed in a spectrum taken by the Si-CCD (Fig. 5(a)). Based on an excitation power-dependent measurement (Fig. 4(b)), the emission could be assigned to an exciton transition by determining the slope of the intensity increase in a logarithmic plot.[15] Before starting the correlation measurement, the QD emission line was scanned using both of the SPADs in a narrow spectral range. By fitting a Gaussian distribution to the measured spectrum, the single-photon counting rate of 34 250 counts/s and the background emission of 2770 counts/s can be determined (Fig. 4(a)). The second order correlation $g^{(2)}(0) = 0.37$ at zero time delay was derived from fitting an exponential function of $g^{(2)}(\tau) = 1 - a\, e^{-|\tau|/\tau_0}$ to the experimentally obtained temporal correlation (Fig. 5(b)).

The low $g^{(2)}(0)$ proves single-photon emission of the device. Nevertheless, the origin of a non-zero $g^{(2)}(0)$ should be discussed at this point. To this end, the amount of background that takes part in the correlation function can be estimated by the offset b and the maximum intensity s of the QD emission line detected with the SPADs. The background leads to a constant offset $g_{bg} = (2\,b\,s + b^2)/(b + s)^2 = 0.14$ to the correlation function. This dependency is derived by normalizing the correlation function to the probability

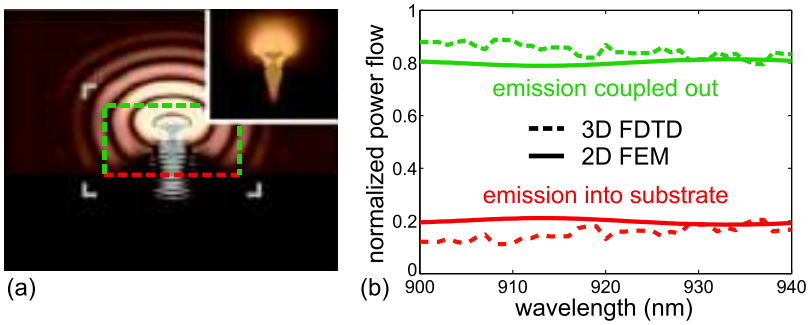

FIG. 3. (a) Illustrated absolute value of Poynting vector from FDTD simulation at the end of simulation time with logarithmic color scale. The inset shows time-integrated values. Gray borders mark the beginning of the absorbing perfectly matched layers (PMLs); red and green dashed lines indicate surfaces at which the power flow into the substrate and vacuum is calculated, respectively (see text). (b) The spectral power flow from FDTD and FEM simulations show good agreement on out-coupling efficiencies of about 80%–90% over the complete spectrum.

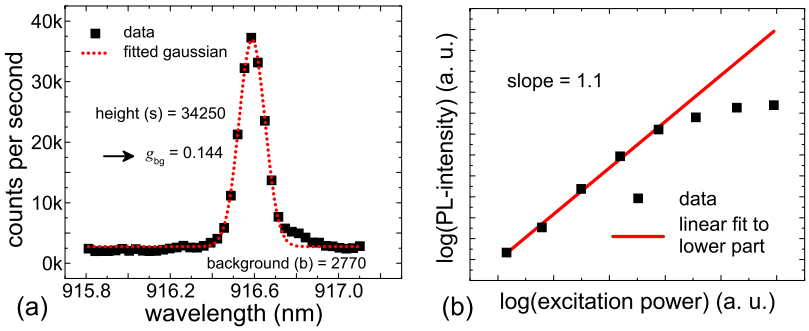

FIG. 4. (a) QD emission line measured with the two SPADs of the HBT set-up. Full width of half maximum is limited by the set opening of the output slit. (b) Excitation power-dependent measurement reveals excitonic nature of QD emission.

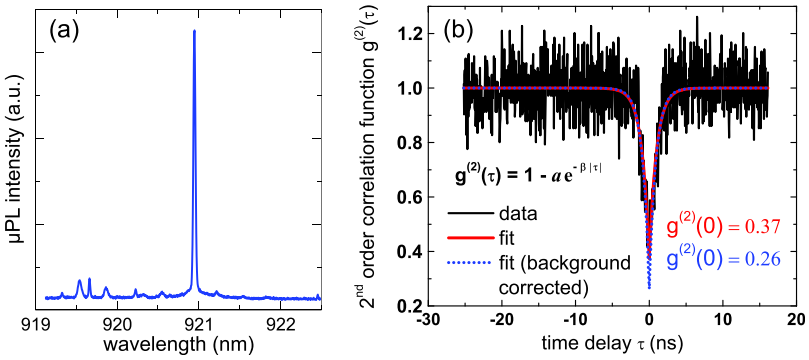

FIG. 5. Emission spectrum of quantum-dot cavity (a) and its second order correlation function (b). Single QD lines can be well separated in the spectrum. The low value of $g^{(2)}(0)$ proves the single-photon character of the emission.

$\Gamma_{\mathrm{bin}} = (b+s)^2\,(\Delta t_{\mathrm{bin}})^2$ that a coincidence appears within the time interval Δt_{bin} of a single bin of the time to amplitude converter. The dark counts of the detectors can be neglected in this case because they are in the range of 10–30 s^{-1} and thus two orders of magnitude below the background observed in the measurement. By subtracting the background point-wise from the measured correlation function and repeating the exponential fit, a $g^{(2)}(0)$ of 0.26 can be calculated. At this point, we want to consider that due to a necessary re-normalization after subtracting the background part point-wise, the change in $g^{(2)}(0)$ is not equal to g_{bg}. The residual signal of the correlation function at zero time delay can be explained by the time resolution of the system, which must be about 360 ps with respect to the width and depth of the anti-bunching dip assuming a Gaussian response. Thus, we can estimate an actual $g^{(2)}(0) = 0.14$ of the devices limited by background emission.

Quantifying the efficiency of the device is difficult due to the cw excitation used. On the other hand, comparison with previously published count rates for similar conditions (non-resonant cw excitation, neutral exciton emission, and comparable $g^{(2)}(0)$) allows for classifying. Crucial for the comparison is to experimentally determine the maximum transmittance of the respective optical system. For this measurement, we opened the monochromator slits completely and removed the pinhole from the detection path, in order to avoid intensity losses in the optical path due to imaging errors. Thus, we determined a maximum transmittance of $4.6\% \pm 0.3\%$ at 900 nm. Taking the specified detector efficiency of 30% into account, the emission rate into a numerical aperture of 0.4 can be estimated to be at least 2.5×10^6 photons/s. Compared to measurements in Ref. 1 on the neutral exciton line in resonance with a "state of the art" Bragg-cavity and similar $g^{(2)}(0) = 0.4$, our value is about a factor of 7 lower. The difference may result from the design of the cavities in Ref. 1 to match the numerical aperture of the collecting optics. Nevertheless, considering the manufacturing efforts, the efficiency of our cavities is highly competitive.

Further improvements on the collection efficiency could be realized by enhancing the numerical aperture of the detection optics, e.g., by solid immersion lenses, but of course a more directional emission would be favoured. To this end, we suggest to leave additional upright side walls on top of the reversed pyramids. This could be achieved by an earlier well-defined etch stop (compare Fig. 2 graphs 4 and 5). This cavity would combine the opportunities of the pyramidal facets to reflect light into the upper half space and a "waveguiding" in the upper part that should lead to a lower numerical aperture of the radiation. Furthermore, an index-matched anti-reflection coating on top of the cavity could enhance the directionality and additionally reduce the photonic density of states in the cavity making the device less sensitive to imperfections conditioned by fabrication.

In conclusion, we have experimentally demonstrated that wet-chemically etched micro-pyramids can be utilized to easily access single quantum-dot emission out of a self-assembled ensemble. With low manufacturing efforts, we are able to realize highly efficient single-photon devices. The high count rates on the detectors could be confirmed by 3D FDTD as well as 2D FEM simulations promising extraction efficiencies between about 80% and 90% over a spectral range of 40 nm.

This work has been performed within project A2 of the DFG Research Center for Functional Nanostructures (CFN). It has been further supported by a grant from the Ministry of Science, Research and the Arts of Baden-Württemberg

(Az: 7713.14-300). We further acknowledge support by the Karlsruhe School of Optics and Photonics (KSOP).

[1]S. Strauf, N. G. Stoltz, M. T. Rakher, L. A. Coldren, P. M. Petroff, and D. Bouwmeester, Nat. Photonics **1**, 704 (2007).
[2]T. Heindel, C. Schneider, M. Lermer, S. H. Kwon, T. Braun, S. Reitzenstein, S. Höfling, M. Kamp, and A. Forchel, Appl. Phys. Lett. **96**, 011107 (2010).
[3]G. Ortner, M. Schwab, M. Bayer, R. Pässler, S. Fafard, Z. Wasilewski, P. Hawrylak, and A. Forchel, Phys. Rev. B **72**, 085328 (2005).
[4]M. M. Vogel, S. M. Ulrich, R. Hafenbrak, P. Michler, L. Wang, A. Rastelli, and O. G. Schmidt, Appl. Phys. Lett. **91**, 051904 (2007).
[5]J. Beetz, C. Kistner, M. Lermer, C. Schneider, S. Reitzenstein, S. Höfling, M. Kamp, and A. Forchel, Appl. Phys. Lett. **98**, 191111 (2011).
[6]W. Löffler, M. Hetterich, C. Mauser, S. Li, T. Passow, and H. Kalt, Appl. Phys. Lett. **90**, 232105 (2007).
[7]S. Jeppesen, M. S. Miller, D. Hessman, B. Kowalski, I. Maximov, and L. Samuelson, Appl. Phys. Lett. **68**, 2228 (1996).
[8]M. Helfrich, D. Hu, J. Hendrickson, M. Gehl, D. Rülke, R. Gröger, D. Litvinov, S. Linden, M. Wegener, D. Gerthsen, T. Schimmel, M. Hetterich, H. Kalt, G. Khitrova, H. Gibbs, and D. Schaadt, J. Cryst. Growth **323**, 187 (2011).
[9]C. Schneider, T. Heindel, A. Huggenberger, T. A. Niederstrasser, S. Reitzenstein, A. Forchel, S. Höfling, and M. Kamp, Appl. Phys. Lett. **100**, 091108 (2012).
[10]V. Cambel, D. Gregušová, and R. Kúdela, J. Appl. Phys. **94**, 4643 (2003).
[11]F. M. Weber, M. Karl, J. Lupaca-Schomber, W. Löffler, S. Li, T. Passow, J. Hawecker, D. Gerthsen, H. Kalt, and M. Hetterich, Appl. Phys. Lett. **90**, 161104 (2007).
[12]M. Karl, T. Beck, S. Li, H. Kalt, and M. Hetterich, Appl. Phys. Lett. **92**, 231105 (2008).
[13]D. Rülke, M. Karl, D. Hu, D. Schaadt, H. Kalt, and M. Hetterich, J. Cryst. Growth **324**, 259 (2011).
[14]W. Sheng and J.-P. Leburton, Appl. Phys. Lett. **80**, 2755 (2002).
[15]K. Brunner, G. Abstreiter, G. Böhm, G. Tränkle, and G. Weimann, Phys. Rev. Lett. **73**, 1138 (1994).